Effects of Salt on the Thermal Stability of Human Plasma High-Density Lipoprotein †

ARTICLE *in* BIOCHEMISTRY · MAY 2006

Impact Factor: 3.02 · DOI: 10.1021/bi0524565 · Source: PubMed

3 AUTHORS, INCLUDING:

Olga. Gursky
Boston University
63 PUBLICATIONS **1,331** CITATIONS

SEE PROFILE

Effects of Salt on the Thermal Stability of Human Plasma High-Density Lipoprotein†

Shobini Jayaraman,* Donald L. Gantz, and Olga Gursky

Department of Physiology and Biophysics, Boston University School of Medicine, Boston, Massachusetts 02118

Received December 1, 2005; Revised Manuscript Received January 23, 2006

ABSTRACT: High-density lipoproteins (HDL) mediate cholesterol removal and thereby protect against atherosclerosis. Mature spherical HDL contain the apolar lipid core and polar surface of proteins and phospholipids. Earlier, we showed that the structural integrity of HDL is modulated by kinetic barriers that prevent spontaneous protein dissociation and lipoprotein fusion and rupture. To determine the role of electrostatic interactions in the kinetic stability of mature HDL, here we analyze the effects of salt and pH on their thermal denaturation. In low-salt buffer at pH 5.7−7.7, HDL are highly thermostable. Increasing the salt concentration from 0 to 0.3 M NaCl causes low-temperature shifts in the calorimetric HDL transitions of up to −14 °C. This salt-induced destabilization leads to protein unfolding below 100 °C, facilitating the first Arrhenius analysis of HDL denaturation by circular dichroism spectroscopy. In 150 mM NaCl, two kinetic phases in HDL protein unfolding are observed: a faster phase with an activation energy $E_{a,fast} \leq 15$ kcal/mol and a slower phase with an $E_{a,slow} = 50 \pm 7$ kcal/mol. Gel electrophoresis and electron microscopic data suggest that the faster phase involves partial protein unfolding but no significant protein dissociation or changes in HDL size, while the slower phase involves complete protein unfolding, partial protein dissociation, and HDL fusion. Hence, the slower phase may resemble HDL remodeling and fusion by plasma enzymes during metabolism. Analysis of the effects of various salts, sucrose, and pH suggests that HDL destabilization by salt results from ionic screening of favorable short-range electrostatic interactions such as salt bridges. Consequently, electrostatic interactions significantly contribute to the high thermostability of HDL in low-salt solutions.

Lipoproteins are complexes of proteins and lipids that are central in the transport and metabolism of cholesterol. Plasma lipoproteins, including high-density, low-density, and very low-density lipoproteins (HDL,[1] LDL, and VLDL), differ in size, composition, and metabolic properties. HDL are dubbed "good cholesterol" because plasma levels of HDL and its major protein, apolipoprotein A-1 (apoA-1, 28 kDa), correlate inversely with the probability of developing coronary artery disease (*1*, *2*). This protective action is due to cholesterol transport by HDL from peripheral tissues to the liver for removal (*3*) and to antioxidant and antiinflammatory effects of HDL (*2*, *4*, *5*).

Human HDL are heterogeneous particles ($d = 9-12$ nm) containing several protein and 150−300 lipid molecules (*2*, *6*). Nascent HDL are phospholipid bilayer disks containing two to four copies of apoA-1 that is thought to adopt an extended α-helical "double-belt" conformation around the disk perimeter (*6*−*9*) (Figure 1). Mature HDL are spherical particles containing an apolar core of cholesterol esters and triglycerides and a polar surface comprised of a cholesterol-containing phospholipid monolayer and two to four copies of apoA-1 and other proteins (Figure 1). During metabolism, HDL exchange their protein and lipid constituents with other lipoproteins and are extensively remodeled by plasma enzymes (*6*, *10*), yet they maintain their structural integrity that is necessary for lipoprotein functions. Our goal is to elucidate the energetic basis of this structural integrity.

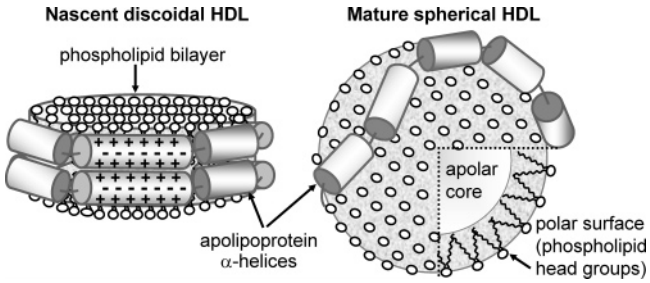

FIGURE 1: Cartoon representation of discoidal and spherical HDL. Lipid packing in spherical HDL is shown in the cross section (bottom right). The charge distribution in apolipoprotein α-helices (shown in the two front helices on discoidal HDL) facilitates formation of multiple intra- and interhelical salt bridges between oppositely charged groups, most of which are located three or four positions apart within the helix. Such a charge distribution may also cause repulsion among the closely spaced basic residues located in the low-dielectric environment at the lipid−water interface (*21*).

HDL proteins such as apoA-1 and apoA-2 (which comprise 70 and 20% of HDL protein content, respectively) belong to a family of exchangeable apolipoproteins. During metabolism, these water-soluble proteins transfer among

† This work was supported by NIH Grants GM 67260 and HL26355.

* To whom correspondence should be addressed: Department of Physiology and Biophysics, Boston University School of Medicine, W329, 715 Albany St., Boston, MA 02118. Phone: (617) 638-7894. Fax: (617) 638-4041. E-mail: shobini@bu.edu.

[1] Abbreviations: HDL, high-density lipoprotein(s); LDL, low-density lipoprotein(s); VLDL, very low-density lipoprotein(s); apo, apolipoprotein; CD, circular dichroism; DSC, differential scanning calorimetry; EM, electron microscopy; *T*-jump, temperature jump.

10.1021/bi0524565 CCC: $33.50
Published on Web 03/15/2006

lipoproteins via the lipid-poor or lipid-free state (*11*), but their predominant state is in association with lipoproteins. Exchangeable apolipoproteins bind to the phospholipid surface via the large apolar faces of their amphipathic α-helices (*12*). These helices, which are formed of 11/22-mer tandem amino acid sequence repeats, have an unusually high content of charged residues (30−40%) with a distinct radial distribution: acidic groups are located in the middle of the polar helical face and basic groups flank the apolar face (Figure 1). Hence, the basic groups can form hydrophobic interactions with the lipid acyl chains as well as electrostatic interactions with the phospholipid headgroups (*7*, *13*). In addition to binding to phospholipid surface (*14*−*16*), electrostatic interactions have been implicated in essential apolipoprotein functions such as interactions with lipoprotein receptors and transporters and activation of lipolytic enzymes that are central in lipoprotein metabolism (*17*−*21*). Furthermore, the high content and distinct distribution of charged residues (most of which are separated from the oppositely charged group by three or four positions within the helix) facilitate formation of extensive intra- and interhelical salt bridges. Such salt bridges have been proposed to stabilize the double-belt apolipoprotein conformation on discoidal HDL (*7*, *8*, *22*); this notion was tested experimentally using reconstituted HDL disks (*21*). The role of electrostatic interactions in the stability of spherical HDL, which have more diverse and less well-defined protein conformations, is unclear and is in the focus of this work.

HDL stability has been the subject of intense investigation for more than 30 years. With few exceptions (*23*−*26*), these studies used equilibrium thermodynamic methods, and only a few reports addressed electrostatic effects (*27*−*29*). Our recent analysis of discoidal and spherical HDL (*30*−*32*) and LDL (*33*) established a kinetic mechanism of lipoprotein stabilization. We and others showed that exposure of HDL to denaturing conditions causes protein dissociation (*23*, *34*) and fusion of the protein-depleted particles that compensates for the reduction in their polar surface (*30*, *31*). Furthermore, under strongly denaturing conditions, spherical lipoproteins rupture and release their apolar core lipids that coalesce into large droplets (*31*−*33*). Chemical denaturation studies showed that HDL fusion and rupture are thermodynamically irreversible and involve high free energy barriers [$\Delta G^* \cong$ 17 kcal/mol (*31*)]. Such kinetic barriers may confer particle stability, prevent unregulated interconversions among HDL subclasses, and thereby modulate HDL metabolism. Here, we address the role of electrostatic interactions in the kinetic stability of human HDL.

Our recent studies of the electrostatic effects in model discoidal HDL suggested an inverse correlation between lipoprotein stability and salt sensitivity: salt stabilizes relatively unstable complexes but destabilizes more stable complexes (*21*). We proposed that the short-range Coulombic interactions significantly contribute to the stability of discoidal HDL, with a net effect that may be favorable (in more stable complexes) or unfavorable (in less stable complexes); hence, more stable lipoproteins are destabilized by ionic screening, while less stable lipoproteins are stabilized by it. Here we extend this hypothesis to spherical HDL. To probe for the first time the role of electrostatic interactions in the kinetic stability of spherical HDL, we perform thermal denaturation of mature human HDL in a broad range of solvent ionic conditions (from 5 mM to 1.5 M salt, pH 5.7−7.7). The results support our hypothesis and show that spherical plasma HDL are highly thermostable in low-salt solutions but are destabilized at near-physiologic salt concentrations due to ionic screening of favorable electrostatic interactions. Our results also reveal two kinetic phases in thermal denaturation of HDL. The fast phase, which involves partial unfolding but not dissociation of HDL proteins, may reflect the protein plasticity that is necessary for adaptation to particles of different sizes. The slow phase, which involves protein dissociation and HDL fusion, may resemble metabolic HDL remodeling in plasma.

MATERIALS AND METHODS

Lipoprotein Preparation. All experiments were performed using single-donor HDL that were isolated from the EDTA-treated plasma of four healthy volunteer donors by density gradient ultracentrifugation in the density range of 1.08−1.12 g/mL (35). The sample purity was 95%, as assessed by size and density agarose gel electrophoresis. The HDL solution was dialyzed against 10 mM sodium phosphate buffer containing 0.05% NaN_3 and 0.25 mM NaEDTA (pH 7.7) (which is a standard buffer used throughout this work) and was stored in the dark at 4 °C; studies were also done with HDL in a buffer with a similar composition at pH 5.7. The HDL stock was diluted with a buffered salt solution to the final salt concentration of 0.01−1.5 M and a protein concentration of 1−4 mg/mL (for calorimetric and electron microscopic studies) or 20 μg/mL (for spectroscopic studies). Transition temperatures determined in these studies were independent of HDL concentration in the range that was explored (0.02−4 mg/mL protein). The HDL stock was used in 2 weeks during which no changes in the protein conformation or particle stability were detected by spectroscopy or calorimetry, no protein degradation was detected by SDS gel electrophoresis, and no particle decomposition was detected by nondenaturing gel electrophoresis. HDL fractionation into subclasses was not done in this work since our unpublished chemical denaturation studies suggested no large differences between the unfolding kinetics of HDL_2 and HDL_3.

Differential Scanning Calorimetry (DSC). Excess heat capacity, $C_p(T)$, was recorded from HDL solutions of 3−4 mg/mL protein concentration using an upgraded Microcal MC-2 differential scanning microcalorimeter as described previously (*32*). The data were recorded during heating from 10 to 115 °C at a rate of 90 °C/h, followed by rapid cooling and incubation at 5 °C prior to the recording of the next scan. ORIGIN was used for the data collection, processing, and display.

Circular Dichroism (CD) Spectroscopy. CD data were recorded using AVIV 62DS and AVIV 215 spectrometers with thermoelectric temperature control. Far-UV CD spectra and kinetic and melting data were recorded from HDL samples with 20 μg/mL protein concentration as described previously (*31*). The melting data, $\Theta_{222}(T)$, were recorded at 222 nm during sample heating and cooling with a 1 °C increment and an accumulation time per data point of 60−300 s, which corresponds to the scan rates of approximately 80−11 °C/h. The kinetics of the thermal denaturation was monitored in the temperature-jump (*T*-jump) experiments in

which the sample was rapidly heated at time t = 0 from 25 °C to higher temperatures, and the time course of the α-helical unfolding was monitored at 222 nm as described previously (*31*). Following the buffer baseline subtraction, the CD data were normalized to protein concentration and were expressed as a mean residue ellipticity, [Θ].

Kinetic Analysis. The rates of thermal unfolding of HDL proteins were determined by fitting the CD data recorded in *T*-jump experiments to the multiexponential function

$$\Theta_{222}(T) = A_1 \exp(-\tau_1/t) + A_2 \exp(-\tau_2/t) + ...$$

where A_1 and A_2 are the amplitudes of the kinetic phases and τ_1 and τ_2 are the exponential relaxation times that are the inverse of the reaction rates ($k = 1/\tau$). Since HDL denaturation is irreversible, the reaction rates approximate the unfolding rates. The kinetics of thermal unfolding of HDL proteins was analyzed using an Arrhenius model as described previously (*30*). Briefly, the relaxation times τ at 80−95 °C were determined by fitting the $\Theta_{222}(T)$ data recorded in *T*-jumps from 25 to 80−95 °C, and the activation energy E_a for each kinetic phase was determined from the slope of the Arrhenius plot (ln τ vs $1/T$).

Electron Microscopy (EM). HDL samples subjected to various thermal treatments were visualized by negative staining EM. Images were recorded in a CM12 transmission electron microscope and processed as described previously (*31*). Analysis of the particle size distribution was carried out using PHOTOSHOP graphics with EXCEL; ∼800 particles per image were used.

Nondenaturing Gradient Gel Electrophoresis and Western Blotting. Gel electrophoresis of intact and thermally treated HDL was carried out by using a 5 to 16% polyacrylamide gradient gel. The gel was run at 200 V for 1 h on a Hoefer SE260 mini-vertical apparatus and was stained with Imperial protein stain. In addition, a precast 8 to 25% gradient gel (PHAST system, Pharmacia) was used. Particle diameters were assessed from comparison with protein markers (purchased from Amersham Biosciences) with known Stokes radii: thyroglobulin (660 kDa, 17 nm), ferritin (440 kDa, 12.2 nm), bovine liver catalase (232 kDa, 10.4 nm), bovine heart lactate dehydrogenase (140 kDa, 8.2 nm), and bovine serum albumin (66 kDa, 7.1 nm). Particle sizes were confirmed by EM measurements.

For Western blotting, samples were loaded on native polyacrylamide gels. The proteins were separated for 1 h at 200 V and 22 °C and were transferred to a PVDF membrane for 1 h (100 V and 22 °C). The membrane was blocked for 1 h in Tris-buffered saline/casein blocking buffer. The blots were then probed with antibodies for apoA-1 and apoA-2 in blocking buffer for 1 h. Blots were washed three times for 10 min each and were visualized using the ECL system (NEN Life Science Products). All experiments in this study were repeated three to six times to ensure reproducibility.

RESULTS

Effects of Salt on the Calorimetric Transitions in HDL. At 25 °C in 10 mM sodium phosphate (pH 7.7), increasing the salt concentration from 0 to 1.5 M NaCl has no detectable effect on the size or morphology of intact HDL (visualized by negative staining EM), on the secondary structure of HDL proteins (monitored by far-UV CD), or on the packing of their aromatic groups (monitored by near-UV CD and Trp fluorescence, data not shown). However, addition of salt leads to large changes in HDL stability, which is evident from the heat capacity data, $C_p(T)$, of intact HDL containing 0−500 mM NaCl. Figure 2A (black line) shows DSC data recorded for an HDL solution of 4 mg/mL protein concentration in buffer at pH 7.7 upon heating from 5 to 115 °C at a rate of 90 °C/h. In 0 M NaCl, two distinct calorimetric transitions are observed: a broad peak centered at $T_1 \cong 90$ °C and a sharp peak at $T_2 = 112$ °C. The broad peak involves apoA-1 dissociation (*34*) and HDL fusion (*32*), while the sharp peak is attributed to apoA-2 dissociation (*34*) followed by HDL rupture and coalescence of the apolar core lipids into droplets (32).

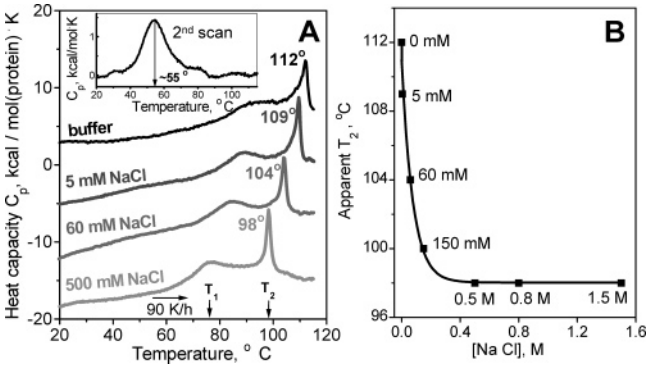

FIGURE 2: Effect of NaCl on the calorimetric transitions in human plasma HDL. HDL samples containing 4 mg/mL protein, 10 mM standard buffer at pH 7.7, and 0−1.5 M NaCl were heated from 5 to 115 °C at a rate of 90 °C/h, and excess heat capacity was recorded by DSC. (A) $C_p(T)$ data at various NaCl concentrations. The data in 0.3−1.5 M NaCl closely overlap. Peak temperatures T_1 and T_2 are indicated by arrows; the values of T_2 are shown near the peaks. The data recorded from the same HDL pool at identical salt concentrations at pH 5.7 and 7.7 closely overlap. The inset shows a second consecutive scan from the same HDL sample in standard buffer; consecutive scans recorded in 0−1.5 M NaCl closely overlap. DSC data recorded of HDL at pH 5.7 and 7.7 under otherwise identical conditions closely overlap. (B) Apparent T_2 of the second calorimetric transition (that involves apoA-2 dissociation and HDL rupture) as a function of NaCl concentration. The solid line shows single-exponential data fitting.

Large low-temperature shifts in both calorimetric transitions are observed with an increase in NaCl concentration from 0 to 500 mM (Figure 2A, gray lines). These shifts are particularly pronounced at millimolar salt concentrations but are saturated at ∼0.2−0.3 M salt, as illustrated in the plot of the apparent temperature T_2 of HDL rupture as a function of NaCl concentration (Figure 2B). The single-exponential character of this function (Figure 2B, solid line) is typical of the electrostatic screening by diffuse counterions (*36*); this function usually levels off at molar salt concentrations where hydrophobic effect of salt becomes predominant. At ion concentrations of ≤0.1 M, the effects of salt on macromolecular stability are dominated by electrostatic interactions (*36*, *37*), suggesting that HDL destabilization by salt is mainly an electrostatic effect.

For single-donor HDL from the same pool, the reproducibility of the peak temperature T_2 is better than 1 °C, yet for HDL from different donors, T_2 measured in low-salt solutions upon heating at 90 °C/h may vary from 106 to 114 °C, which may possibly result from the different content of anionic lipids. Despite this variation, in ≥0.3 M NaCl, HDL from different plasma pools show similar T_2 values of ≅98 °C;

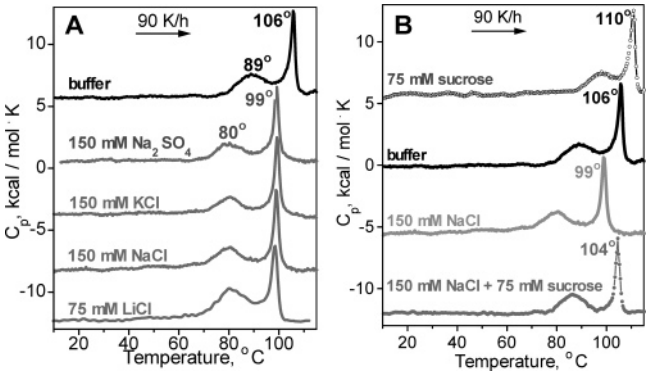

FIGURE 3: Effects of salts and sucrose on HDL stability monitored by DSC. Heat capacity $C_p(T)$ was recorded upon heating at a rate of 90 °C/h of HDL samples (4 mg/mL protein, standard buffer, pH 7.7) that contain 0−150 mM various salts (A) and/or 75 mM sucrose (B). Peak temperatures are indicated.

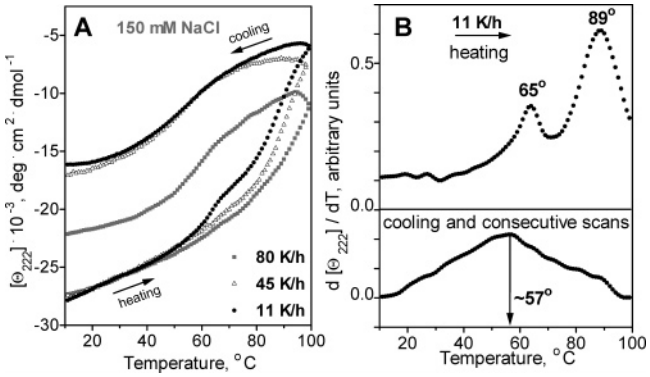

FIGURE 4: Thermal unfolding of HDL proteins monitored by far-UV CD at 222 nm. (A) Effects of scan rate on the melting curves. The $\Theta_{222}(T)$ data were recorded from intact HDL (20 μg/mL protein, 150 mM NaCl in standard buffer at pH 7.7) upon heating and cooling from 2 to 98 °C at a rate of 80 (gray squares), 45 (white triangles), or 11 °C/h (black circles). Cooling curves and consecutive heating and cooling data recorded from the same HDL sample fully overlap similar data recorded at pH 5.7 (not shown) under otherwise identical conditions. (B) First derivative, $d[\Theta_{222}(T)]/dT$, of the heating data (top) and cooling data (bottom) that were recorded at 11 °C/h from HDL in 150 mM NaCl (panel A, black circles). Peak temperatures are indicated.

one possible explanation is that the electrostatic interactions are largely screened at near-physiological salt concentrations and hence do not significantly contribute to the differences in the stability of HDL from different pools.

Calorimetric HDL transitions are irreversible (*31*, *34*), which is evident from the repetitive DSC scans recorded from the same sample during heating from 5 to 115 °C (Figure 2A, inset). These scans show a broad peak centered near 55 °C that reflects the unfolding of dissociated apoA-1 (*34*). In contrast to HDL transitions observed in the first scan, the apoA-1 unfolding observed in the second scan and consecutive scans is independent of the scan rate or of the salt concentration in the range that was explored (0−1.5 M NaCl). This is consistent with the observation that the secondary structure and stability of lipid-free HDL proteins, apoA-1 and apoA-2, remain invariant in 10^{-5} to 1 M salt (*21*). Thus, salt-induced destabilization is observed in HDL but not in its isolated protein moieties.

To test the effects of different salts on HDL stability, DSC data were recorded from HDL solutions containing Na_2PO_4, Na_2SO_4, KCl, NaCl, or LiCl. Figure 3A shows that identical concentrations of different salts induced similar low-temperature shifts in the calorimetric transitions. The only exception is LiCl which is particularly destabilizing; for example, 75 mM LiCl causes a decrease in T_2 similar to that caused by 150 mM NaCl, KCl, or Na_2SO_4 (Figure 3A). Except for Li^+, the effects of salt on HDL stability are not specific to a particular mono- or divalent anion or monovalent cation and do not clearly correlate with the ionic position in the Hoffmeister series. This provides additional evidence for the electrostatic rather than the hydrophobic effect of salt as a driving force for HDL destabilization.

To further test the role of the hydrophobic effect on HDL stability, we compared the effects of salt and sucrose on the calorimetric transitions. In contrast to salt, sucrose reduces water activity but not electrostatic interactions. The $C_p(T)$ data in panels A and B of Figure 3 were recorded from a pool of particularly unstable HDL [T_2 = 106 °C in 10 mM sodium phosphate buffer (pH 7.7) at a scan rate of 90 °C/h], which facilitated direct observation of the effect of sucrose on T_2; HDL from other pools exhibited similar trends. The data in Figure 3B show that, in contrast to low-temperature shifts in HDL transitions observed in 150 mM NaCl (T_2 = 99 °C), a high-temperature shift is detected in 75 mM sucrose (T_2 = 110 °C), even though these solutions have similar water activity. Consequently, HDL destabilization by salt cannot result from the hydrophobic effect. Interestingly, in the presence of both 150 mM NaCl and 75 mM sucrose, the transition temperature T_2 = 104 °C is an average between the values measured in 150 mM NaCl (99 °C) and 75 mM sucrose (110 °C); this suggests that the effects of salt and sucrose are additive and hence occur independently (Figure 3B). In summary, HDL stabilization by sucrose is likely due to the hydrophobic effect, while HDL destabilization by salt is predominantly electrostatic.

Thermal Unfolding of HDL Proteins Monitored by Far-UV CD. To test whether the heat-induced HDL fusion and rupture, which were observed previously by DSC and EM (*32*), involve protein unfolding, the far-UV CD signal at 222 nm, $\Theta_{222}(T)$, was recorded upon HDL heating and cooling from 5 to 98 °C at a rate of 11 or 80 °C/h. In low-salt buffer, the CD melting data of intact HDL show only partial, low-cooperativity, largely reversible α-helical unfolding upon heating to 98 °C (*32* and references cited therein). In contrast, in 150 mM NaCl or other salts, the unfolding shifts to lower temperatures, becomes more complete, and shows hysteresis, especially at slow scan rates, indicating thermodynamic irreversibility (Figure 4A). Importantly, the $\Theta_{222}(T)$ data in Figure 4A show that reducing the scan rate from 80 to 11 °C/h causes a low-temperature shift in the heating curves of approximately −10 °C. Such a scan rate dependence, which was also observed in discoidal HDL (*30*, *38*) and in spherical plasma LDL (*33*), is a hallmark of slow irreversible transitions with high activation energy (*39*).

Analysis of the shapes of the CD melting curves was facilitated by utilization of long data accumulation times at slow scan rates (5 min/K at a scan rate of 11 °C/h) leading to a low noise level in these data. The $\Theta_{222}(T)$ heating curves recorded at 11 °C/h of HDL in 150 mM NaCl [Figure 4A (●)] or other salts suggest two consecutive transitions centered near T_1 = 65 °C and T_2 = 89 °C, as indicated by the peak positions in the first-derivative function $d[\Theta_{222}(T)]/$

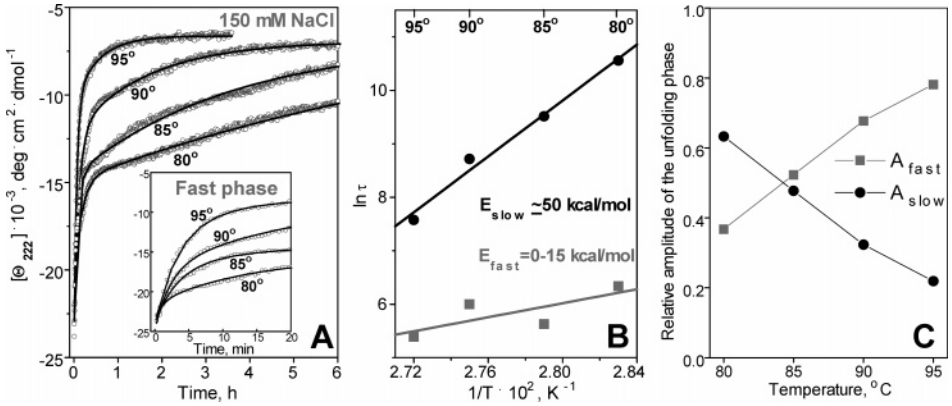

FIGURE 5: Unfolding kinetics of HDL proteins monitored in *T*-jumps by CD at 222 nm. (A) Time course of HDL protein unfolding in 150 mM NaCl. Sample conditions are the same as those described in the legend of Figure 2. The unfolding was triggered at time zero by a rapid increase in temperature from 25 to 80−95 °C; the final temperatures are indicated. Fitting of the $\Theta_{222}(T)$ data by double exponentials (solid lines) suggests two kinetic phases that occur on the time scale of minutes (fast) and hours (slow). The inset shows the initial portion of the data showing the fast unfolding phase. (B) Arrhenius plots (ln τ vs $1/T$) for τ_{fast} and τ_{slow} determined from the double-exponential fitting of the $\Theta_{222}(T)$ traces in panel A. Fitting of the Arrhenius plots for τ_{fast} and τ_{slow} by linear functions (solid lines) suggests that the activation energies for the two kinetic phases are as follows: $E_{a,fast} = 0-15$ kcal/mol and $E_{a,slow} = 50 \pm 7$ kcal/mol. The accuracy of these estimates incorporates the fitting errors and the deviations among the four data sets recorded for single-donor HDL from four different donors. (C) Relative amplitudes A_{fast} and A_{slow} of the two kinetic phases in HDL protein unfolding as a function of temperature. The amplitudes are expressed as a fraction of the total loss in the magnitude of the CD signal at 222 nm during heat unfolding (A).

d*T* (Figure 4B, top). These CD transitions recorded at a scan rate of 11 °C/h correlate with the DSC data recorded at a rate of 90 °C/h in 150 mM NaCl (Figure 3). In fact, CD melting curves shift by ~10 °C when the heating rate is increased from 11 to 80 °C/h (Figure 4A); thus, at 90 °C/h, the two CD transitions are expected to shift to approximately $T_1 \cong 75$ °C and $T_2 \cong 99$ °C. This is in good agreement with the peak temperatures $T_1 \cong 80$ °C and $T_2 = 99$ °C (T_2) observed by DSC for HDL fusion and rupture at 90 °C/h in 150 mM NaCl (Figure 3). Consequently, the two unfolding transitions observed by CD correspond to the HDL transitions observed by DSC.

In contrast to the heating curve of intact HDL, the CD cooling curve shows one broad sigmoidal transition centered near 57 °C [Figure 4A (●) and Figure 4B (bottom)]. This CD transition is reversible, since it remains invariant upon repetitive heating and cooling of the same sample and is independent of the scan rate. It clearly correlates with the second DSC scan of HDL showing a reversible transition around 55 °C (Figure 2A, inset) that reflects reversible folding and unfolding of dissociated apoA-1 in solution (*31*, *34*). In summary, the two irreversible heat unfolding transitions in intact HDL observed by far-UV CD correspond to the calorimetric transitions and involve apolipoprotein dissociation and consequent HDL fusion and rupture; furthermore, the single reversible transition observed in the cooling CD curve and in repetitive CD and DSC scans reflects folding and unfolding of dissociated apoA-1.

Thermal Unfolding Kinetics of HDL Proteins. Destabilization at near-physiological salt concentrations, which causes complete HDL protein unfolding below 100 °C (Figure 4A), was used to perform the first kinetic analysis of thermal denaturation of plasma HDL. The time course of the HDL protein unfolding in 150 mM NaCl, which was triggered by a rapid temperature increase (*T*-jump) at time zero from 25 to 80−95 °C, was monitored by CD at 222 nm. Exponential fitting of the $\Theta_{222}(T)$ data (Figure 5A, solid lines) suggests two unfolding phases: a faster phase with an exponential relaxation time τ_{fast} of ~5 min and a slower phase with a τ_{slow} of hours (the exact values of τ_{fast} and τ_{slow} are donor-dependent). Arrhenius plots (ln τ vs $1/T$) for these two phases are linear (Figure 5B) with slopes corresponding to the following activation energies (enthalpies): $E_{a,slow} = 50 \pm 7$ kcal/mol and $E_{a,fast} \cong 0-15$ kcal/mol; the accuracy of these estimates incorporates the fitting errors and the deviations among the data sets recorded for single-donor HDL from four different donors.

To determine the physical origin of the two unfolding phases, we used nondenaturing gel electrophoresis to analyze the time course of the heat-induced protein dissociation and lipoprotein fusion. The HDL sample containing 150 mM NaCl was incubated at 85 °C, and the aliquots taken at different times during incubation were analyzed by using a 5 to 16% gradient polyacrylamide gel (Figure 6A) or an 8 to 25% PHAST gradient gel (not shown). Intact HDL show two distinct bands on the 8 to 25% gel corresponding to two major subclasses: HDL_3 ($d = 7-8$ nm, two apoA-1 molecules per particle) and HDL_2 ($d = 9-13$ nm, three to four apoA-1 molecules per particle); these bands appear merged on the 5 to 16% gel (lane 1 in Figure 6A), which may result from nonuniform gradient formation by a manual method. After incubation for 2−5 min at 85 °C (which corresponds to an exponential relaxation time $\tau_{fast} = 5$ min for the fast unfolding phase determined by CD), no changes in the particle size are observed (lanes 2 and 3 in Figure 6A). Thus, the fast unfolding phase is not accompanied by any detectable protein dissociation or changes in lipoprotein size. In contrast, incubation for 15 min to 3 h (which encompasses $\tau_{slow} = 75$ min for the slow unfolding phase at 85 °C) leads to the gradual disappearance of the intact-size HDL and to protein redistribution among two fractions: one fraction corresponds to lipid-free or lipid-poor protein dissociated from HDL and another to enlarged particles with sizes ranging from ~12 to 18 nm that are apparent products of HDL fusion (lanes 4−12 in Figure 6A). Further incubation for up to 12 h does not lead to any additional changes (data not shown). Western blotting showed concomitant dissociation of apoA-1 and apoA-2 during the slow phase (data not

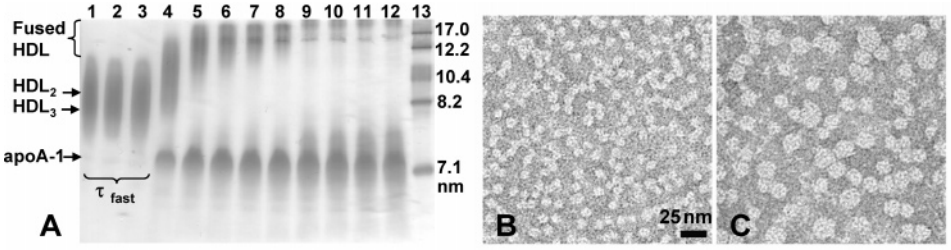

FIGURE 6: Time course of the heat-induced protein dissociation and HDL fusion monitored by nondenaturing gel electrophoresis (A) and negative staining electron microscopy (B and C). Each HDL sample (1 mg/mL protein, 150 mM NaCl, standard buffer, pH 7.7) was subjected to a temperature jump from 25 to 85 °C; exponential relaxation times for the protein unfolding in such a *T*-jump determined by far-UV CD are as follows: $\tau_{fast} = 5$ min and $\tau_{slow} = 75$ min. (A) Nondenaturing 5 to 16% polyacrylamide gradient gel electrophoresis showing intact HDL (lane 1), HDL incubated at 85 °C for 2 (lane 2), 5 (lane 3), 15 (lane 4), 30 (lane 5), 45 (lane 6), 60 (lane 7), 75 (lane 8), 100 (lane 9), 120 (lane 10), 150 (lane 11), and 180 min (lane 12), and high-molecular weight standards with Stokes diameters in nanometers (lane 13). Negative staining EM of intact HDL (B) and of HDL incubated at 85 °C for 75 min (C). Sample conditions are the same as those described for panel A.

shown). Thus, the fast phase involves partial protein unfolding but no dissociation or HDL remodeling, whereas the slow phase involves complete protein unfolding, dissociation of a fraction of apoA-1 and apoA-2 from HDL, and concomitant HDL fusion.

To further test the origin of the two kinetic phases, we used negative staining EM to monitor the time course of the heat-induced changes in lipoprotein morphology. The HDL sample containing 150 mM NaCl was incubated at 85 °C, and the aliquots taken at different times during incubation were visualized. Intact HDL appear as round-shaped particles with an average diameter of 9.9 ± 0.2 nm, which is typical for humans (Figure 6B). After incubation for 5 min at 85 °C (which corresponds to τ_{fast}), no changes in the particle size are observed by EM (data not shown), which is consistent with the results of nondenaturing gel electrophoresis (lanes 2 and 3 in Figure 6A). In contrast, incubation for 75 min (τ_{slow}) leads to an increase in the average particle diameter to 15.5 ± 0.2 nm due to fusion (Figure 6C). This result is consistent with gel electrophoresis of this sample showing enlarged particles ranging in size from ~12 to 18 nm (lane 8, Figure 6A). Taken together, our far-UV CD, gel electrophoresis, and EM data show that the fast kinetic phase involves partial unfolding of the HDL-anchored protein but no lipoprotein remodeling, while the slow kinetic phase involves complete protein unfolding, partial dissociation of apoA-1 and apoA-2 from HDL, and concomitant lipoprotein fusion.

The two kinetic phases in HDL protein unfolding have comparable CD amplitudes (Figure 5C), suggesting that apoA-1 (which constitutes ~70% of HDL helical structure) significantly contributes to each of these unfolding phases. One possibility is the presence of two distinct comparable size populations of apoA-1 on HDL differing in conformation and/or interactions with apoA-2 (*40* and references cited therein). Another possibility is that different parts of the apoA-1 molecule dissociate and unfold at different rates: unfolding of the N-terminal and central part (which have relatively low lipid binding affinity) may contribute to the fast unfolding phase, followed by unfolding of the more tightly bound C-terminal part and protein dissociation during the slow phase.

Our results suggest that one population of apoA-1 (or one part of the apoA-1 molecule, probably its N-domain) unfolds relatively fast at high temperatures, implicating a relatively small free energy barrier (ΔG^*_{fast}). This barrier ($\Delta G^*_{fast} = \Delta H^*_{fast} - T\Delta S^*_{fast}$) has a small enthalpic component ($\Delta H^*_{fast} \cong E_{a,fast} \leq 15$ kcal/mol) (Figure 5B), which implies relatively small transient disruption of protein and lipid packing interactions; this is consistent with the absence of any significant protein dissociation or changes in the lipoprotein morphology detected in this phase. In contrast, unfolding of the remaining protein fraction (or of the remaining part of apoA-1, probably its C-domain) is relatively slow and hence involves a higher free energy barrier [$\Delta G^*_{slow} - \Delta G^*_{fast} = RT \ln(\tau_{slow}/\tau_{fast})$]. The high activation energy of the slow phase ($E_{a,slow} \cong 50$ kcal/mol) reflects transient disruption of extensive interactions during protein dissociation and HDL fusion observed in this phase (Figure 6). This value is comparable to the activation energy of 60−70 kcal/mol reported for desorption of apoA-1 from model discoidal HDL (*25*, *38*).

In summary, far-UV CD, gel electrophoresis, and EM data suggest two alternatives. In the first scenario, there are two distinct populations of apoA-1 on HDL: one population can readily unfold without dissociating from HDL, while the other forms extensive contacts on HDL in its folded state and is essential for the integrity of the particle. The difference between the two populations may be due to the conformational heterogeneity of apoA-1 on HDL, to different modes of apoA-1−lipid interactions (*40* and references cited therein), and/or to interactions of a fraction of apoA-1 molecules with apoA-2 that reportedly prevents dissociation of apoA-1 from HDL (*41*). Alternatively, our results suggest sequential unfolding and dissociation of the putative N- and C-domains in apoA-1 (*42*).

DISCUSSION

Our results show that mature human HDL in low-salt solutions are highly thermostable: heating at 90 °C/h leads to protein dissociation and unfolding and consequent HDL fusion and rupture at $T_1 \cong 90$ °C and $T_2 \cong 106-115$ °C (Figures 2A and 3, black lines). Slow rates of these transitions [which occur on a time scale of minutes to hours (Figure 5A) as compared to the nano- to millisecond time scale typical for helix-to-coil transition in solution (*43*)] are consistent with the slow transition rates observed in chemical denaturation of HDL and confirm that HDL are stabilized by high free energy barriers (*30*). Although kinetic stability has been proposed to provide a universal natural strategy

for stabilizing macromolecular complexes (*44*), to our knowledge, this is the first report of a kinetically stable macromolecular complex that is highly thermostable.

Since HDL are heterogeneous complexes that can exchange their protein and lipid constituents, factors other than specific packing of apolar groups must contribute to their high thermostability. Our results reveal that electrostatic interactions are among these factors. Several lines of evidence indicate that the destabilizing effect of salt on HDL observed by DSC and far-UV CD (Figures 2A and 4A) is due to ionic screening of favorable electrostatic interactions. First, at salt concentrations that destabilize HDL ($10^{-2}-10^{-1}$ M, Figure 2B), the effects of salt on macromolecular stability are dominated by ionic screening; in contrast, specific ion binding usually occurs at lower salt concentrations ($<10^{-3}$ M), while the hydrophobic effect of salt becomes predominant at higher concentrations (>0.1 M) (*37*, *45*). Exponential saturation of the salt effect on HDL stability (Figure 2B) is also consistent with Debye−Huckel screening by diffuse counterions (*36*). Furthermore, opposite effects of salt (destabilizing) and sucrose (stabilizing) argue against the hydrophobic effect of salt as a driving force for HDL destabilization (Figure 3B). The lack of Hoffmeister-type effects on HDL stability also argues against the hydrophobic effect of salt, while comparable effects of different salt ions on HDL stability suggest nonspecific ionic interactions (Figure 3A). Taken together, these results indicate that HDL destabilization by salt is due to ionic screening of favorable electrostatic interactions.

What is the nature of these favorable interactions? Since changes in pH from 5.7 to 7.7, and hence in the net charge on HDL, have no significant effect on HDL stability [as indicated by the overlapping DSC and far-UV CD data recorded at pH 5.7 (not shown) and pH 7.7 (Figures 2−4)], these interactions must be short-range. Furthermore, since charge−charge interactions are most susceptible to ionic screening (*36*, *37*) and since most HDL charges are located on the protein, it is likely that the short-range Coulombic protein−protein interactions such as salt bridges significantly enhance HDL stability. Similarly, thermophilic proteins, which have a high charged residue content, are stabilized by extensive networks of highly optimized surface salt bridges (*46*−*49*), particularly intrahelical salt bridges (*50*). A high content of charged residues and their specific distribution in apolipoprotein α-helices may also facilitate formation of stabilizing intra- and interhelical salt bridge networks on the HDL surface. Additional HDL stabilization may result from favorable interactions between the basic protein groups and anionic phospholipids that are present in small amounts on HDL and possibly contribute to the donor-specific differences in HDL stability observed in low-salt solutions. At near-physiological salt concentrations, these favorable electrostatic interactions are largely screened out and may not significantly contribute to HDL stability.

In contrast to spherical plasma HDL, model discoidal HDL have moderate thermal stability that may be enhanced or diminished by salt ions depending on the composition of the particle (*21*). One possible explanation of this difference in the thermal stability and salt sensitivity of HDL disks and spheres is that the protein α-helices in discoidal HDL are mainly confined to the disk perimeter while the protein conformation at the surface of spherical HDL is probably less constrained (*6*−*9*) (Figure 1). This may alleviate the repulsion among the closely spaced basic residues located in the low-dielectric environment at the lipid−water interface (*21*) and lead to a highly optimized surface charge distribution that stabilizes spherical particles. Partially buried surface salt bridges, which may be different in HDL disks and spheres, may also contribute to the differences in stability and salt sensitivity of these particles. In addition, anionic phospholipids, which are present in small amounts in plasma HDL but not in our disk preparations, may form stabilizing interactions with the basic apolipoprotein residues and hence contribute to the high thermostability of human plasma HDL.

In summary, our results reveal that high thermal stability of human plasma HDL in low-salt solutions is due, in part, to optimized electrostatic interactions. Screening of these favorable interactions by salt ions destabilizes HDL and facilitates the first CD spectroscopic analysis of HDL protein unfolding below 100 °C. The two kinetic phases detected by this analysis at near-physiological salt concentrations can be explained by sequential unfolding and dissociation of the N- and C-terminal portions of apoA-1 on HDL or by the presence of two distinct populations of apoA-1 on HDL. The N-domain of apoA-1 (or protein subpopulation) that gives rise to the fast unfolding phase can undergo a change in its conformation while remaining anchored to HDL. Such conformational plasticity of apoA-1 is thought to be responsible for its ability to adapt to different-sized HDL and for providing structural integrity to HDL during metabolic remodeling (*51*). The C-domain of apoA-1 (or protein subpopulation) that gives rise to the slow unfolding phase forms extensive contacts on HDL, which is evident from the high activation energy of its dissociation and unfolding ($E_{a,slow} \cong 50$ kcal/mol); this high activation energy also has a contribution from the transient disruption of lipid−lipid interactions during HDL fusion that is observed in this phase (Figure 6). Similarly, a high activation energy may be involved in HDL remodeling by plasma enzymes, since this remodeling often involves proteolysis, phospholipid lipolysis, or apolar lipid transfer which creates an imbalance between the polar HDL surface and its apolar core, leading to HDL fusion. Heat- or denaturant-induced protein dissociation from HDL may lead to a similar imbalance and fusion (*32*) and, hence, may mimic aspects of enzymatic HDL remodeling.

The results of this study further support an inverse correlation between lipoprotein stability and salt sensitivity: highly thermostable complexes such as spherical plasma HDL are strongly destabilized by salt, while less stable model discoidal HDL are progressively stabilized by salt (*21*). A similar inverse correlation between salt sensitivity and thermal stability was observed in several families of mesophilic, thermophilic, and superthermophilic protein homologues, including cold shock proteins, chemotaxis proteins, and ribonuclease H (*37*). Our results suggest that this correlation may be a general electrostatic phenomenon that applies not only to thermodynamically stable globular proteins but also to kinetically stable macromolecular complexes such as HDL.

ACKNOWLEDGMENT

We are indebted to Dr. Haya Herscovitz for help with Western blotting, to Cheryl England and Michael Gigliotti

for HDL isolation, and to Xuan Gao for help with particle size analysis.

REFERENCES

1. Gordon, T., Castelli, W. P., Hjortland, M. C., Kannel, W. B., and Dawber, T. R. (1977) High-density lipoprotein as a protective factor against coronary heart disease. The Framingham Study, *Am. J. Med. 62* (5), 707−714.
2. Asztalos, B. F. (2004) High-density lipoprotein metabolism and progression of atherosclerosis: New insights from the HDL Atherosclerosis Treatment Study, *Curr. Opin. Cardiol. 19* (4), 385−391.
3. Fielding, C. J., and Fielding, P. E. (1995) Molecular physiology of reverse cholesterol transport, *J. Lipid Res. 36* (2), 211−228.
4. Nicholls, S. J., Rye, K. A., and Barter, P. J. (2005) High-density lipoproteins as therapeutic targets, *Curr. Opin. Lipidol. 16* (3), 345−349.
5. Barter, P. J. (2005) Cardioprotective effects of high-density lipoproteins: The evidence strengthens, *Arterioscler. Thromb. Vasc. Biol. 25* (7), 1305−1306.
6. Lund-Katz, S., Liu, L., Thuahnai, S. T., and Phillips, M. C. (2003) High-density lipoprotein structure, *Front. Biosci. 8*, 1044−1054.
7. Segrest, J. P., Jones, M. K., Klon, A. E., Sheldahl, C. J., Hellinger, M., De Loof, H., and Harvey, S. C. (1999) A detailed molecular belt model for apolipoprotein A-I in discoidal high-density lipoprotein, *J. Biol. Chem. 274* (45), 31755−31758.
8. Brouillette, C. G., Anantharamaiah, G. M., Engler, J. A., and Borhani, D. W. (2001) Structural models of human apolipoprotein A-I: A critical analysis and review, *Biochim. Biophys. Acta 1531* (1−2), 4−46.
9. Davidson, W. S., and Silva, R. A. (2005) Apolipoprotein structural organization in high-density lipoproteins: Belts, bundles, hinges and hairpins, *Curr. Opin. Lipidol. 16* (3), 295−300.
10. Barter, P. J. (2002) The regulation and remodelling of HDL by plasma factors, *Atheroscler. Suppl. 3* (4), 39−47.
11. Rye, K. A., and Barter, P. J. (2004) Formation and metabolism of prebeta-migrating, lipid-poor apolipoprotein A-I, *Arterioscler. Thromb. Vasc. Biol. 24* (3), 421−428.
12. Segrest, J. P., Jones, M. K., De Loof, H., Brouillette, C. G., Venkatachalapathi, Y. V., and Anantharamaiah, G. M. (1992) The amphipathic helix in the exchangeable apolipoproteins: A review of secondary structure and function, *J. Lipid Res. 33* (2), 141−166.
13. Mishra, V. K., Palgunachari, M. N., Segrest, J. P., and Anantharamaiah, G. M. (1994) Interactions of synthetic peptide analogs of the class A amphipathic helix with lipids. Evidence for the snorkel hypothesis, *J. Biol. Chem. 269* (10), 7185−7191.
14. Kanellis, P., Romans, A. Y., Johnson, B. J., Kercret, H., Chiovetti, R., Jr., Allen, T. M., and Segrest, J. P. (1980) Studies of synthetic peptide analogs of the amphipathic helix. Effect of charged amino acid residue topography on lipid affinity, *J. Biol. Chem. 255* (23), 11464−11472.
15. Epand, R. M., Surewicz, W. K., Hughes, D. W., Mantsch, H., Segrest, J. P., Allen, T. M., and Anantharamaiah, G. M. (1989) Properties of lipid complexes with amphipathic helix-forming peptides. Role of distribution of peptide charges, *J. Biol. Chem. 264* (8), 4628−4635.
16. Lecompte, M. F., Bras, A. C., Dousset, N., Portas, I., Salvayre, R., and Ayrault-Jarrier, M. (1998) Binding steps of apolipoprotein A-I with phospholipid monolayers: Adsorption and penetration, *Biochemistry 37* (46), 16165−16171.
17. Desrumaux, C., Athias, A., Masson, D., Gambert, P., Lallemant, C., and Lagrost, L. (1998) Influence of the electrostatic charge of lipoprotein particles on the activity of the human plasma phospholipid transfer protein, *J. Lipid Res. 39* (1), 131−142.
18. Masson, D., Athias, A., and Lagrost, L. (1996) Evidence for electronegativity of plasma high-density lipoprotein-3 as one major determinant of human cholesteryl ester transfer protein activity, *J. Lipid Res. 37* (7), 1579−1590.
19. Sparks, D. L., Frank, P. G., and Neville, T. A. (1998) Effect of the surface lipid composition of reconstituted LPA-I on apolipoprotein A-I structure and lecithin: Cholesterol acyltransferase activity, *Biochim. Biophys. Acta 1390* (2), 160−172.
20. Alexander, E. T., Bhat, S., Thomas, M. J., Weinberg, R. B., Cook, V. R., Bharadwaj, M. S., and Sorci-Thomas, M. (2005) Apolipoprotein A-I helix 6 negatively charged residues attenuate lecithin-cholesterol acyltransferase (LCAT) reactivity, *Biochemistry 44* (14), 5409−5419.
21. Benjwal, S., Jayaraman, S., and Gursky, O. (2005) Electrostatic effects on the stability of discoidal high-density lipoproteins, *Biochemistry 44* (30), 10218−10226.
22. Klon, A. E., Segrest, J. P., and Harvey, S. C. (2002) Molecular dynamics simulations on discoidal HDL particles suggest a mechanism for rotation in the apoA-I belt model, *J. Mol. Biol. 324* (4), 703−721.
23. Reijngoud, D. J., and Phillips, M. C. (1982) Mechanism of dissociation of human apolipoprotein A-I from complexes with dimyristoylphosphatidylcholine as studied by guanidine hydrochloride denaturation, *Biochemistry 21*, 2969−2976.
24. Epand, R. M. (1982) The apparent preferential interaction of human plasma high-density apolipoprotein A-I with gel-state phospholipids, *Biochim. Biophys. Acta 712*, 146−151.
25. Reijngoud, D. J., and Phillips, M. C. (1984) Mechanism of dissociation of human apolipoproteins A-I, A-II and C from complexes with dimyristoylphosphatidylcholine as studied by thermal denaturation, *Biochemistry 23*, 726−734.
26. Surewicz, W. K., Epand, R. M., Pownall, H. J., and Hui, S. W. (1986) Human apolipoprotein A-I forms thermally stable complexes with anionic but not with zwitterionic phospholipids, *J. Biol. Chem. 34*, 16191−16197.
27. Sparks, D. L., Lund-Katz, S., and Phillips, M. C. (1992) The charge and structural stability of apolipoprotein A-I in discoidal and spherical recombinant high-density lipoprotein particles, *J. Biol. Chem. 267* (36), 25839−25847.
28. Sparks, D. L., Davidson, W. S., Lund-Katz, S., and Phillips, M. C. (1993) Effect of cholesterol on the charge and structure of apolipoprotein A-I in recombinant high-density lipoprotein particles, *J. Biol. Chem. 268* (31), 23250−23257.
29. Davidson, W. S., Sparks, D. L., Lund-Katz, S., and Phillips, M. C. (1994) The molecular basis for the difference in charge between pre-beta- and alpha-migrating high-density lipoproteins, *J. Biol. Chem. 269* (12), 8959−8965.
30. Gursky, O., Ranjana, and Gantz, D. L. (2002) Complex of human apolipoprotein C-1 with phospholipid: Thermodynamic or kinetic stability? *Biochemistry 41*, 7373−7384.
31. Mehta, R., Gantz, D. L., and Gursky, O. (2002) Human plasma high-density lipoproteins are stabilized by kinetic factors, *J. Mol. Biol. 328*, 183−192.
32. Jayaraman, S., Gantz, D. L., and Gursky, O. (2004) Poly(ethylene glycol)-induced fusion and destabilization of human plasma high-density lipoproteins, *Biochemistry 43* (18), 5520−5531.
33. Jayaraman, S., Gantz, D. L., and Gursky, O. (2005) Structural basis for thermal stability of human low-density lipoprotein, *Biochemistry 44* (10), 3965−3971.
34. Tall, A. R., Deckelbaum, R. J., Small, D. M., and Shipley, G. G. (1977) Thermal behavior of human plasma high-density lipoprotein, *Biochim. Biophys. Acta 487* (1), 145−153.
35. Schumaker, V. N., and Puppione, D. L. (1986) Sequential flotation ultracentrifugation, *Methods Enzymol. 128*, 155−170.
36. Perez-Jimenez, R., Godoy-Ruiz, R., Ibarra-Molero, B., and Sanchez-Ruiz, J. M. (2004) The efficiency of different salts to screen charge interactions in proteins: A Hofmeister effect? *Biophys. J. 86* (4), 2414−2429.
37. Dominy, B. N., Perl, D., Schmid, F. X., and Brooks, C. L. (2002) The effects of ionic strength on protein stability: The cold shock protein family, *J. Mol. Biol. 319* (2), 541−554.
38. Jayaraman, S., Gantz, D. L., and Gursky, O. (2005) Kinetic stabilization and fusion of apolipoprotein A-2: DMPC disks: Comparison with apoA-1 and apoC-1, *Biophys. J. 88* (4), 2907−2918.
39. Sanchez-Ruiz, J. M., Lopez-Lacomba, J. L., Cortijo, M., and Mateo, P. L. (1988) Differential scanning calorimetry of the irreversible thermal denaturation of thermolysin, *Biochemistry 27* (5), 1648−1652.
40. Curtiss, L. K., Bonnet, D. J., and Rye, K. A. (2000) The conformation of apolipoprotein A-I in high-density lipoproteins is influenced by core lipid composition and particle size: A surface plasmon resonance study, *Biochemistry 39* (19), 5712−5721.
41. Rye, K. A., Wee, K., Curtiss, L. K., Bonnet, D. J., and Barter, P. J. (2003) Apolipoprotein A-II inhibits high-density lipoprotein remodeling and lipid-poor apolipoprotein A-I formation, *J. Biol. Chem. 278* (25), 22530−22536.
42. Saito, H., Dhanasekaran, P., Nguyen, D., Holvoet, P., Lund-Katz, S., and Phillips, M. C. (2003) Domain structure and lipid

interactions in human apolipoproteins A-I and E, a general model, *J. Biol. Chem. 278* (27), 23227−23232.
43. Kubelka, J., Hofrichter, J., and Eaton, W. A. (2004) The protein folding 'speed limit', *Curr. Opin. Struct. Biol. 14* (1), 76−88.
44. Plaza del Pino, I. M., Ibarra-Molero, B., and Sanchez-Ruiz, J. M. (2000) Lower kinetic limit to protein thermal stability: A proposal regarding protein stability in vivo and its relation with misfolding diseases, *Proteins 40*, 58−70.
45. Arakawa, T., and Timasheff, S. N. (1984) Mechanism of protein salting in and salting out by divalent cation salts: Balance between hydration and salt binding, *Biochemistry 23* (25), 5912−5923.
46. Sanchez-Ruiz, J. M., and Makhatadze, G. I. (2001) To charge or not to charge? *Trends Biotechnol. 19* (4), 132−135.
47. Kumar, S., and Nussinov, R. (2002) Relationship between ion pair geometries and electrostatic strengths in proteins, *Biophys. J. 83* (3), 1595−1612.
48. Makhatadze, G. I., Loladze, V. V., Ermolenko, D. N., Chen, X., and Thomas, S. T. (2003) Contribution of surface salt bridges to protein stability: Guidelines for protein engineering, *J. Mol. Biol. 327* (5), 1135−1148.
49. Dominy, B. N., Minoux, H., and Brooks, C. L. (2004) An electrostatic basis for the stability of thermophilic proteins, *Proteins 57* (1), 128−141.
50. Das, R., and Gerstein, M. (2000) The stability of thermophilic proteins: A study based on comprehensive genome comparison, *Funct. Integr. Genomics 1* (1), 76−88.
51. Wang, L., Atkinson, D., and Small, D. M. (2005) The interfacial properties of apoA-I and an amphipathic α-helix consensus peptide of exchangeable apolipoproteins at the triolein/water interface, *J. Biol. Chem. 280* (6), 4154−4165.

BI0524565